Research article

Fanfan Lu[a], Wending Zhang[a,*], Jiachen Zhang, Min Liu, Lu Zhang, Tianyang Xue, Chao Meng, Feng Gao, Ting Mei* and Jianlin Zhao

Grating-assisted coupling enhancing plasmonic tip nanofocusing illuminated via radial vector beam

https://doi.org/10.1515/nanoph-2019-0329
Received August 25, 2019; revised October 10, 2019; accepted October 25, 2019

Abstract: Tip-enhanced Raman spectroscopy (TERS) is a very useful method to achieve label-free and super-resolution imaging, and the plasmonic tip nanofocusing plays a decisive role for TERS performance. Here, we present a method to enhance the nanofocusing characteristic of a plasmonic tip integrated in a grating near the tip apex. Simulation results show that the grating near the tip apex can significantly improve the electric field intensity of the nanofocusing field compared with a conventional bare tip, under axial excitation of a tightly focused radial vector beam. The electric field enhancement characteristic is quantified in relation with the groove number of grating, excitation wavelength, period of grating, and numerical aperture of the micro-objective (MO). These simulation results could be a good reference to fabricate a plasmonic tip for TERS applications, which is an effective way to promote the development of tip-enhanced near-field optical microscopy.

Keywords: plasmonic tip nanofocusing; radial vector beam; tip-enhanced Raman spectroscopy; surface plasmon polariton.

1 Introduction

In the past two decades, tip-enhanced Raman spectroscopy (TERS) has received extensive attention. The most remarkable feature of TERS technology is that it can provide label-free chemical analysis with nanometer spatial resolution and corresponding topographical imaging [1]. Therefore, as an effective means of analysis, TERS was widely adopted to investigate the biological systems [2], low-dimensional materials [3], single-molecule detection [4], catalysis [5], surface physics [6–8], and so on.

In the application process of TERS technology, the nanofocusing characteristic of the plasmonic tip plays a crucial role. Generally, a sharp metallic tip is used as the plasmonic tip. Under illumination of the external focused light, the field can be compressed to the nanoscale at the tip apex due to the localized surface plasmon resonance effect [9–13]. The enhanced electric field at the tip apex is used to excite and enhance Raman signal within nanoscale.

For the elongated metallic tip commonly used in TERS system, it is generally known that only the electric field component paralleling the axis of the tip can effectively excite the nanofocusing field at the tip apex [14–17]. Thus, it is an effective way to obtain strong TER signals by illuminating the tip apex using a light beam with strong longitudinal field component under tight focusing. In the previous works, it was demonstrated that the metallic tip was axially excited via the focused radial vector beam (RVB) can obtain a higher TER signal than that of the linear polarized beam (LPB) excitation [18–20] because RVB has stronger longitudinal electric field component than that of LPB in case of tight focusing [19].

[a]**Fanfan Lu and Wending Zhang:** These authors contributed equally to this work.
***Corresponding authors: Wending Zhang and Ting Mei,** MOE Key Laboratory of Material Physics and Chemistry Under Extraordinary Conditions and Shaanxi Key Laboratory of Optical Information Technology, School of Science, Northwestern Polytechnical University, Xi'an 710072, China, e-mail: zhangwd@nwpu.edu.cn (W. Zhang); ting.mei@ieee.org (T. Mei). https://orcid.org/0000-0003-1411-1425 (W. Zhang)
Fanfan Lu, Jiachen Zhang, Min Liu, Lu Zhang, Tianyang Xue, Chao Meng and Jianlin Zhao: MOE Key Laboratory of Material Physics and Chemistry Under Extraordinary Conditions and Shaanxi Key Laboratory of Optical Information Technology, School of Science, Northwestern Polytechnical University, Xi'an 710072, China
Feng Gao: MOE Key Laboratory of Weak-Light Nonlinear Photonics, TEDA Applied Physics Institute and School of Physics, Nankai University, Tianjin 300457, China

In addition to achieve electric field enhancement at the tip apex by regulating the polarization of the excitation light, it is also essential to design the shape of the tip to improve the nanofocusing characteristic [21–30]. For example, Raschke et al. introduced a plasmonic tip with a grating written on the tip shaft to significantly reduce background illumination, to achieve high contrast in TERS [21, 22]. Cancado et al. proposed a tip with a single groove carved near the tip apex to tune the resonance wavelength and achieve electric field enhancement, simultaneously [26, 27]. Lu et al. proposed a tip with surface corrugated grating at the tip apex to improve the collection efficiency and the localized field intensity [28]. In the case of z-polarized plane wave side illumination, the localized field intensity near the apex of the tip with surface corrugated grating is about twice as strong as the conventional bare tip.

In this paper, we present a method to enhance the electric field enhancement characteristic of a plasmonic tip with a grating near the apex. Under axial excitation of a tightly focused RVB, the simulation results show that the grating near the tip apex can significantly improve the localized field intensity, which is two orders of magnitude higher than that of the conventional bare tip. Meanwhile, the electric field intensity enhancement characteristic is also quantified in relation with the groove number of grating, excitation wavelength, period of grating, and numerical aperture of the microobjective (MO).

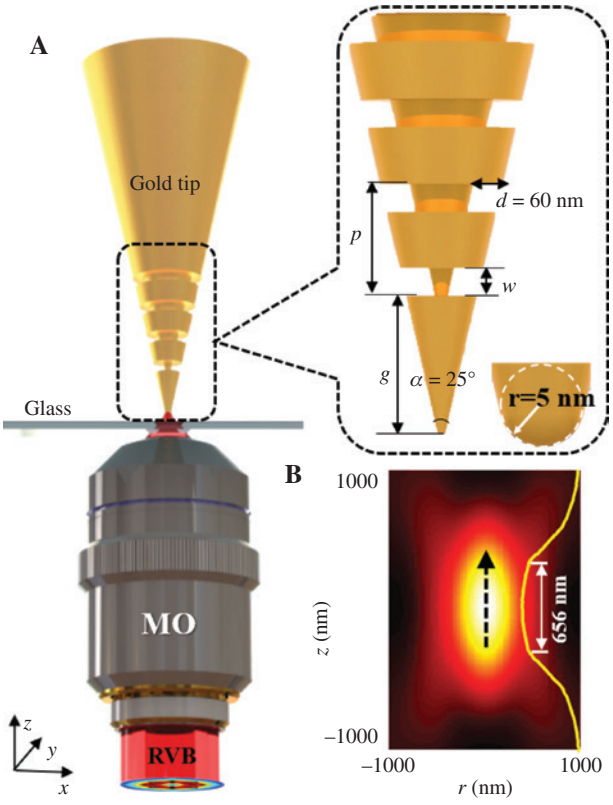

Figure 1: Calculation model of plasmonic tip nanofocusing. (A) Sketch map of the grating-assisted coupling tip nanofocusing axially excited via the tightly focused RVB. Inset is the enlargement of the tip with geometric parameters. (B) Normalized longitudinal electric field intensity distribution of the tightly focused RPB in the r-z plane (NA = 0.9, λ = 633 nm).

2 Methods

Figure 1A is a sketch map of the grating-assisted plasmonic tip axially excited via a tightly focused RVB. Gold (Au) is used as the material of the tip, and the structure parameters of the tip with grating is shown as inset in Figure 1A. A rounded-tip cone with a cone angle $\alpha = 25°$ terminated by a hemisphere with a radius of $r = 5$ nm is used. The distance between the tip-apex and the first groove is g. The period of grating is p varying from 200 nm to 500 nm, the width of grating groove is w, and the depth is $d = 60$ nm. RVB is tightly focused via a MO with high numerical aperture (NA), and then set to propagate along the tip axis to axially excite the plasmonic tip.

Based on the structure parameters of the tip shown as inset in Figure 1A, the 3D finite difference time domain (FDTD Solutions, Lumerical Inc., Vancouver, BC, Canada) method was adopted to calculate the electric field enhancement of the tip under axial excitation of the tightly focused RVB. The permittivity of Au is taken from Johnson and Christy [31]. Non-uniform grid sizes are employed for all calculations to ensure a good tradeoff between accuracy, memory requirements, and simulation time. A uniform grid size of 1 nm is used in the volume 40 nm × 40 nm × 50 nm containing the tip apex and 0.5-nm mesh size around the tip apex, while the other grid size is taken to be less than $\lambda/50$. Because of the rotational symmetry of the tip and the excitation source, the symmetry boundary is used to save the simulation time. The perfectly matched layer (PML) is used as absorption boundary to avoid unphysical reflections around structures. In addition, the PML is placed along the upper cone surface to reduce reflection of SPPs from the upper tip cone boundary [32].

Cylindrical vector beams (CVBs) are vector-beam solutions of Maxwell's wave equation and have axial symmetry in both amplitude and phase [33]. RVB is a type of CVBs, and its polarization is aligned along the radial direction in the transverse plane. Under the condition of tight focusing, based on the Richards-Wolf vector diffraction theory [33, 34], the longitudinal and

transverse electric field components E_z and E_r of RVB can be expressed as

$$E_r = A_0 \int_0^{\alpha} P(\theta)\cos^{1/2}\theta \sin(2\theta) J_1(kr\sin\theta)\exp(ikz\cos\theta)\mathrm{d}\theta \quad (1)$$

$$E_z = 2iA_0 \int_0^{\alpha} P(\theta)\cos^{1/2}\theta \sin^2\theta J_0(kr\sin\theta)\exp(ikz\cos\theta)\mathrm{d}\theta \quad (2)$$

where r and z are the cylindrical coordinates, A_0 is the amplitude, $k=2\pi/\lambda$ is the wave vector, α is the maximal angle determined by NA of the MO, and J_0 and J_1 are the first kind of Bessel function with the orders of 0 and 1. $P(\theta)$ is the pupil function of MO with formation as [35]:

$$P(\theta) = \exp\left[-\beta^2\left(\frac{\sin\theta}{\sin\alpha}\right)^2\right] J_1\left(\frac{2\beta\sin\theta}{\sin\alpha}\right) \quad (3)$$

where $\beta=1$ is the ratio between the pupil radius and the beam waist. The script that solved Eqs. (1) and (2) is written in Matlab code (Matlab, The Math Works, Natick, MA, USA) and imported into the FDTD software. The normalized longitudinal electric field intensity distribution of the focused RVB in r-z plane is shown in Figure 1B.

The electric field intensity enhancement factor is defined as $EF = |E_{loc}|^2/|E_0|^2$, where $|E_{loc}|^2$ is the localized electric field intensity located 1 nm below the tip apex, and $|E_0|^2$ is the incoming electric field intensity of the focused RVB. In addition, the improvement factor $I = EF_{Tip\text{-}Grating}/EF_{Bare\text{-}Tip}$ is defined as the ratio between $EF_{Tip\text{-}Grating}$ induced by the grating-assisted tip and $EF_{Bare\text{-}Tip}$ induced by the bare tip to evaluate the improvement performance of the electric field enhancement characteristic of the grating-assisted tip. The structural parameters of the bare tip are the same as the grating-assisted tip, except for the metallic grating.

3 Results and discussions

3.1 Influence of the tip position in the longitudinal component of RVB on EF

The generation of the localized surface plasmon (LSP) mode at the tip apex is closely related to the polarization direction of the excitation light [19]. When the plasmonic tip is axially excited via the tightly focused RVB, the polarization direction of the longitudinal electric field component, as shown by the arrow in Figure 1B, parallels to the tip axis. Thus, the longitudinal electric component of the focused RVB is the determinant for the generation of LSP mode at the tip apex. In addition, it should be noted that the longitudinal electric field component has a length of ~656 nm along the z-axis. The influence of the tip apex position in the longitudinal electric field component on the enhancement characteristic is first calculated. Figure 2A is the relationship between the tip position and

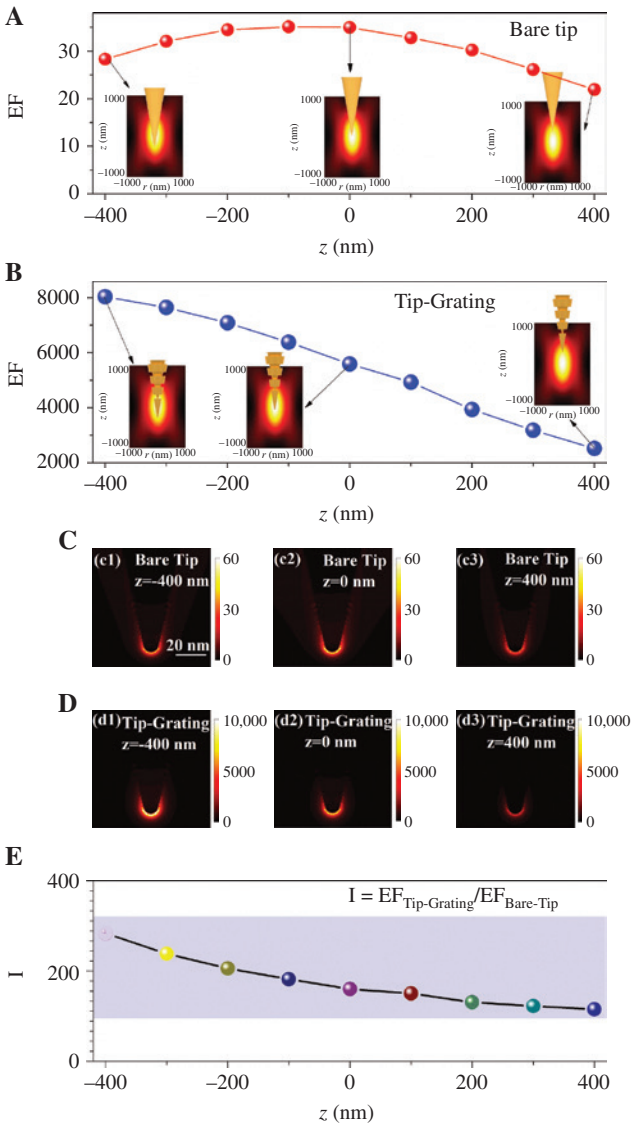

Figure 2: Calculation of electric field enhancement for the tip apex in different positions.
Influence of the position relationship between the tip apex and the longitudinal component of the tightly focused RVB on the EF for bare tip (A) and grating-assisted tip (B). (A, B) Insets are the sketch maps of the tip apex located at the positions of the longitudinal component of RVB. Electric field intensity distributions near the apex of the bare tip (C) and the grating-assisted tip (D) at three tip positions. (E) Ratio of the electric field enhancement factor of the tip with grating to that of the bare tip.

the $EF_{Bare\text{-}Tip}$ of the bare tip axially excited via the focused RVB as shown in Figure 1B. Note that the position of the tip apex in the longitudinal component does affect $EF_{Bare\text{-}Tip}$, and the optimized $EF_{Bare\text{-}Tip} = 35$ can be obtained when the tip apex is located at the center of the longitudinal component, as shown in the middle inset in Figure 2A. Figure 2B is the relationship between the tip position and $EF_{Tip\text{-}Grating}$. Note that the electric field enhancement characteristics of the grating-assisted tip is significantly different from the bare tip. The optimized $EF_{Tip\text{-}Grating} = 8 \times 10^3$ can be obtained when the tip apex is completely wrapped by the longitudinal component of the focused RVB, as shown in the left inset in Figure 2B. As the tip apex moves away from the longitudinal component region, although the $EF_{Tip\text{-}Grating}$ decreases linearly, the $EF_{Tip\text{-}Grating} = 2 \times 10^3$ can still be obtained when the tip apex is located at the top edge of the longitudinal component, as shown in the right inset in Figure 2B.

In addition, to better understand the influence of the tip position on EF, the electric field intensity distributions near the apex of the bare tip and the grating-assisted tip at three positions are shown in Figure 2C and D, respectively. Figure 2E is the ratio of $EF_{Tip\text{-}Grating}$ to $EF_{Bare\text{-}Tip}$. Note that the EF of the grating-assisted tip is two orders of magnitude higher than that of the bare tip in the whole region of the longitudinal component of the focused RVB. It indicates that the grating located near the tip apex can strongly improve the nanofocusing characteristic of the plasmonic tip. For the grating-assisted tip, no matter where the tip in the focus region of RVB is, the EF is still in the magnitude of 10^3, which is strong enough to acquire excellent TERS performance. For convenience, the tip apex is located at the center of the focusing region whether it is a bare tip or a grating-assisted tip in the later calculations.

3.2 Influence of grating groove number on EF

With the parameters of the tip and the excitation light used in Figure 1A, the influences of the grating groove number on the electric field enhancement characteristic of the tip are calculated. Figure 3A is the relationship between EF and the grating groove number. Note that the EF of the grating-assisted tip increases gradually as the groove number increases from $N = 1$ to 6 and remains on the order of ~10^3, which is two orders of magnitude higher than that of the bare tip (EF ~ 30). Figure 3B and C show the electric field intensity distributions near the apex of the bare tip and the grating-assisted tip with $N = 4$, respectively. This phenomenon can be considered as an interference effect between the localized surface plasmons (LSPs) from the tip apex and the surface plasmon polaritons (SPPs) generated from gratings. Using the formalism of the Green's function [36], the electric field underneath the tip apex can be expressed as

$$\mathbf{E}_{total} = \mathbf{E}_0(g) + \mathbf{E}_1 e^{i\varphi_1} + \mathbf{E}_2 e^{i\varphi_2} + \cdots \quad (4)$$

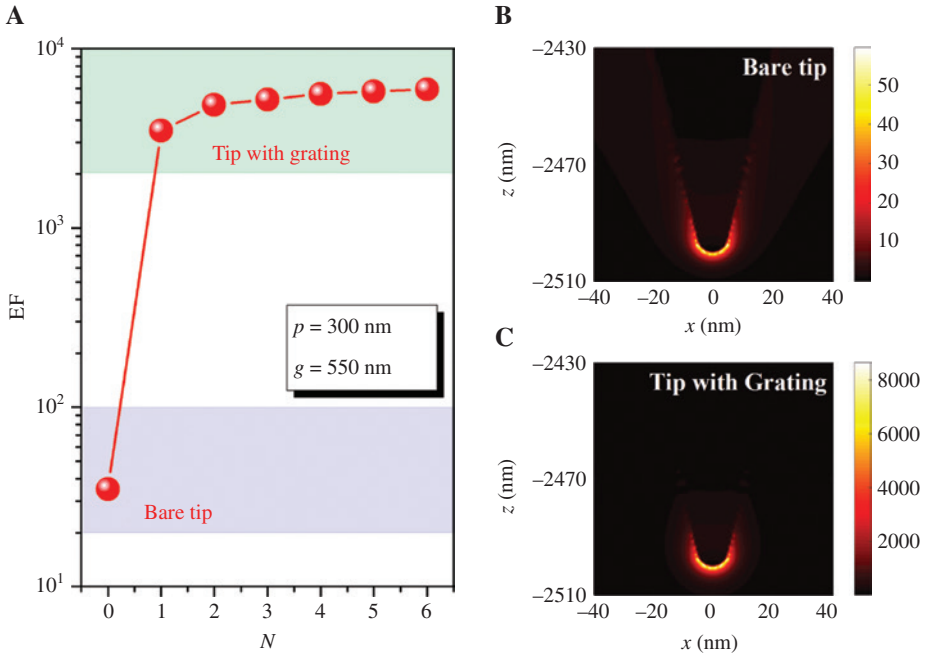

Figure 3: Calculation of electric field enhancement versus grating groove number.
(A) Influence of grating groove number on the EF of the tip. Electric field intensity distributions on the *x*–*z* plane near the apex of the bare tip (B) and the grating-assisted tip with four grooves (C) ($\lambda = 633$ nm, NA = 0.9).

where $\mathbf{E}_0(g)$ is the electric field directly induced by the tip apex and dependent on g, which is the distance from the tip apex and the first grating groove. As for the bare tip, $\mathbf{E}_{total}=\mathbf{E}_0$ ($g=infinity$). $\mathbf{E}_i$ is the electric field generated by the i-th grating groove with an initial phase φ_i, which is determined by the structural parameters. The initial phase φ_i is determined by the optical path of SPPs that propagate along the bare tip and the phase delay at the (i–1)th groove. The initial phase φ_i can be written as

$$\varphi_i = k_{sp}[g+\Sigma(i-1)(p-w)]/\cos(\alpha/2)+\Sigma(i-1)\varphi(w) \quad (5)$$

where k_{sp} is the wave vector of SPPs and $\varphi(w)$ is the phase retardation caused by the grating grooves. This model is similar as the "bull's eyes" metasurface [37], although the scenario in this work is more complicated due to its complex configuration. When all the parameters including geometrical parameters and the wavelength of the incident light are fixed, the initial phase is fixed. Thus, as the number of the grating grooves increases, more contributions from grating are obtained, and EF increases. Because of the limited focusing region and propagation loss, the contributions from the i-th grating groove become smaller, which means that the main contribution to the electric field enhancement is from the tip apex and the first grating groove after tip milling grating. Considering the fabrication process and the field enhancement comprehensively, the groove number $N=4$ is chosen in further simulations.

3.3 Spectral responses of EF for grating parameters

Generally, the grating period for SPP excitation should satisfy the phase-matching condition $k_{sp}=k_0\cos(\alpha/2)\pm n2\pi/p$ [38–41], where k_{sp} is the wave vector of the SPPs (actually, k_{sp} is dependent on the cross-sectional radius of the bare tip, but here, we regard k_{sp} as a constant at different positions due to the small change range of k_{sp} in the grating region [38]), k_0 is the wave vector of the incident light, n is a positive integer ($n=1, 2, 3\ldots$) and $\pm$ represents the SPPs propagating upward and downward. Note that only the downward SPPs could contribute to the electric field enhancement at the tip apex. Thus, the grating period p can be derived as $p=n(1/\lambda_{sp}+\cos(\alpha/2)/\lambda_0)^{-1}$, where λ_0 is the wavelength of the incident light, and λ_{sp} is the wavelength of the SPPs. When $n=1$, the smallest appropriate value of p is obtained.

The influence of the grating period on spectral response is calculated within the wavelength of 600 nm ~ 800 nm, as shown in Figure 4A. Note that the grating period p does not affect the spectral forms of EF, but only slightly affects the magnitude of EF. According to Eq. (4) and the phase-matching condition of the grating, it can be known that the main contribution to $\mathbf{E}_{total}$ is $\mathbf{E}_0(g)$ and $\mathbf{E}_1e^{i\phi 1}$ with g being fixed and $\varphi_1=k_{sp}g$. Thus, the influence of the grating period on EF is inconspicuous, and EF remains in the order of 10^3. The spectral response of the improvement factor I is shown in Figure 4B. Note that the

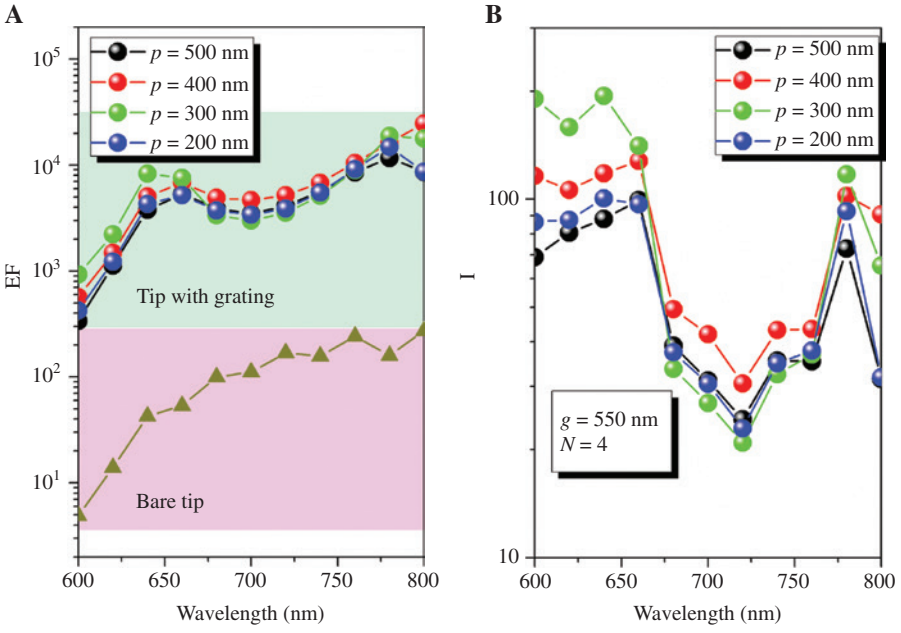

Figure 4: Calculation of electric field enhancement versus grating period.
(A) Spectral responses of the enhancement factor EF and (B) the improvement factor I with different grating periods p.

magnitude of I is affected by the grating period, and better electric field improvement characteristics can be obtained within a short waveband of 600 nm ~ 650 nm.

According to the abovementioned results and discussions, the most critical factor to spectral responses is *g*, the distance from the tip apex to the first groove. Figure 5A shows the effect of *g* on the spectral responses of EF. Note that *g* not only affects the spectra form but also the magnitude of EF. However, EF is still larger than ~10^2 within the wavelength range of 600–800 nm. Figure 5B shows the spectra response of I. The magnitude of I is significantly enhanced with the increase in *g*, which indicates that the spectral response of EF can be optimized by changing *g*.

Based on Eqs. (4) and (5), it can be known that there is still a phase item $\varphi(w)$ caused by the width of the grating groove *w* to influence the interference phenomenon. The grating groove can be regarded as the geometric-phase provider [42, 43]. Thus, it is important to calculate the influence of the groove width *w* on EF and I. Figure 6 shows the spectral responses of EF and I with different grating groove widths *w*. One significant peak is slightly blue shifted, when *w* increases from 50 nm to 150 nm, and EF remains in the order of 10^3 when *w* is in the order of ~10^2 nm. Luo et al. reported a detailed analysis about the dependence of phase retardation on the groove width in a planar metallic plasmonic lens [44–46]. The phase retardation can be tuned by varying the groove width if other parameters are fixed, which is consistent with the calculation results shown in Figure 6.

Apart from the geometric design of the grating, the influence of the focused RVB on the electric field enhancement cannot be ignored. The properties of the focused RVB are almost determined by NA of the MO. Figure 7A and B show the dependence of EF on NA of the bare tip and the grating-assisted tip, respectively. Note that the EF of the bare tip and the grating-assisted tip are all decreased, and the spectral curves are almost identical as NA decreases from 0.9 to 0.7. This result indicates that only the electric field component paralleling to the tip axis and the grating surface can be used to achieve electric field enhancement. With decreasing NA, the proportion of the longitudinal electric filed component of the focused RVB decreases, but the spectral responses remain unchanged, as shown in Figure 7C, which coincides with Figure 7A and B. Figure 7D shows the spectral response of I with different NAs. I decreases with increasing NA, which means that the increase in EF of the grating-assisted tip with NA is less dramatic than that of the bare tip. Nevertheless, even in the case of low NA, the EF of the grating-assisted tip remains in the order of 10^3, which is still much higher than that of the bare tip. It is convenient to expand the TERS system using low NA MO because the low NA MO has a longer working distance.

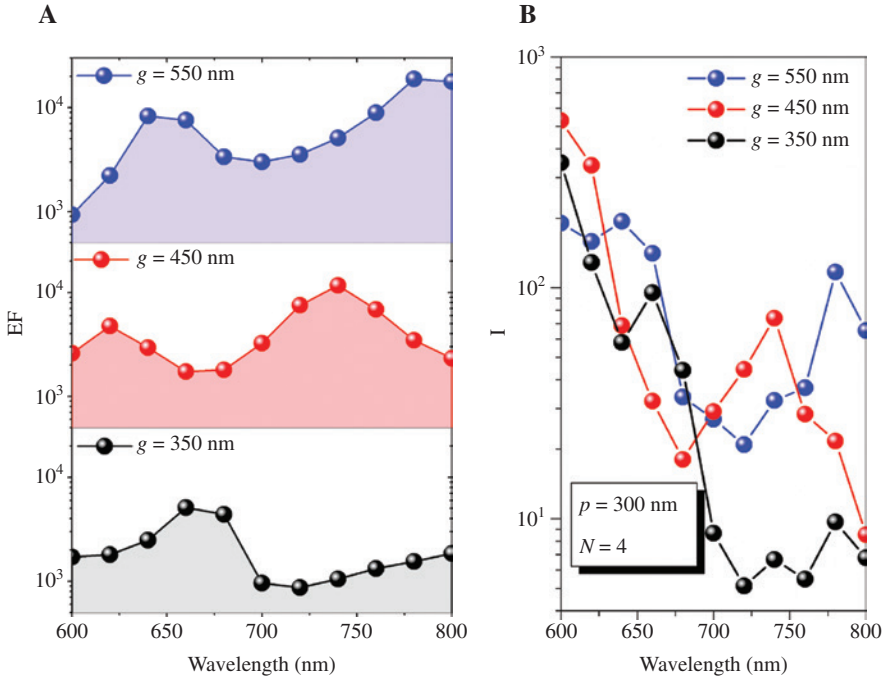

Figure 5: Calculation of electric field enhancement versus the distance from the tip apex to the first groove. Spectral responses of (A) EF and (B) I with different *g*.

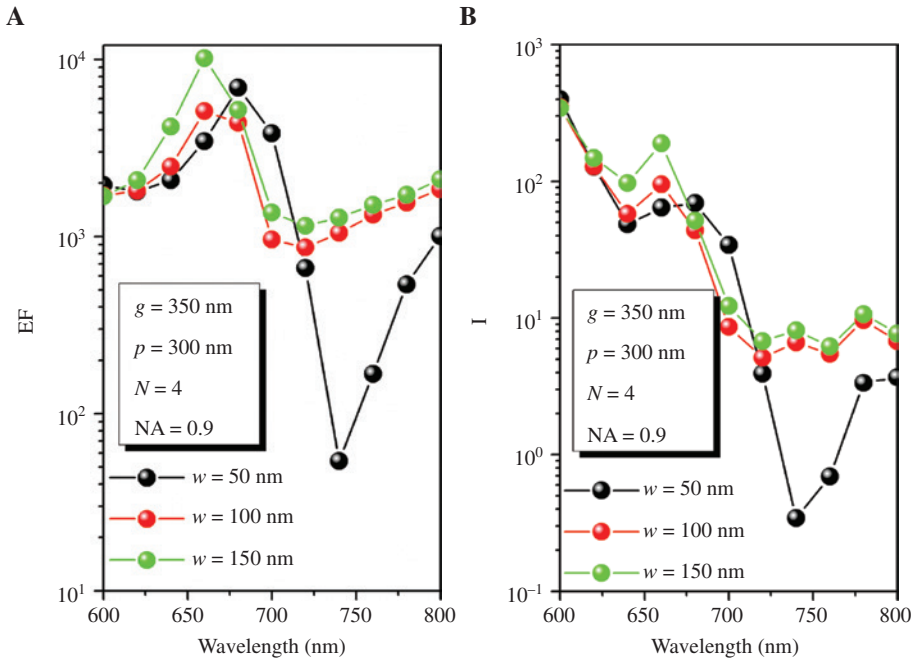

Figure 6: Calculation of electric field enhancement versus grating groove width.
Spectral responses of (A) EF and (B) I with different grating groove widths *w*.

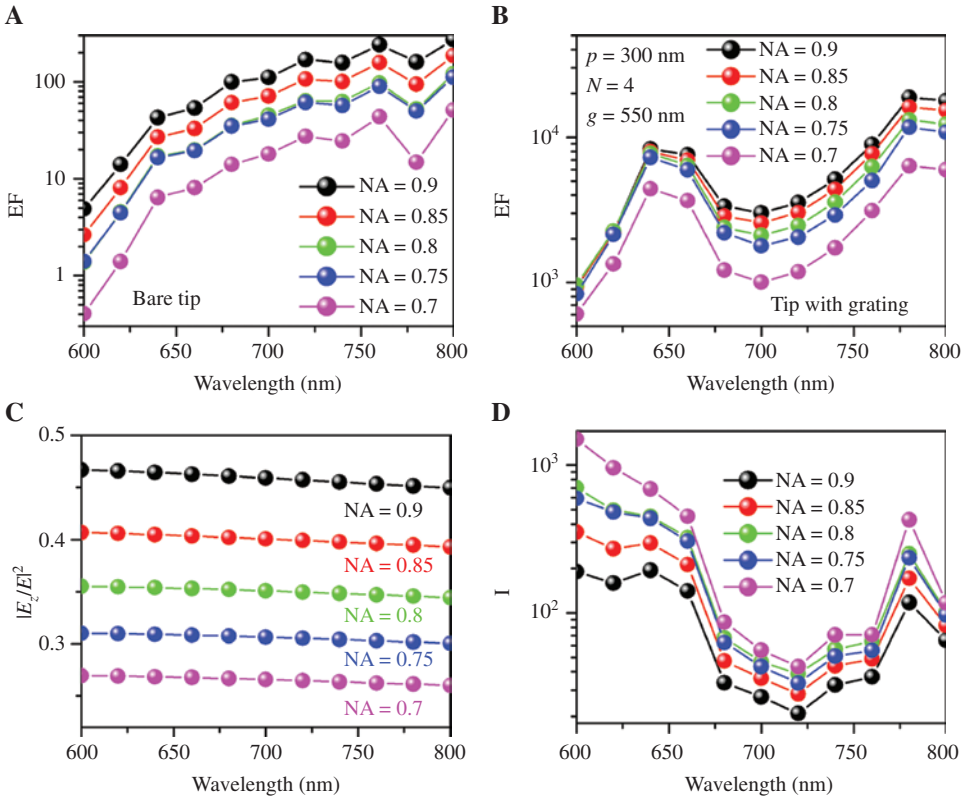

Figure 7: Calculation of electric field enhancement versus different NAs.
Spectral responses of EF of (A) the bare tip and (B) the grating-assisted tip with different NAs. (C) The proportion of longitudinal electric field components with different NAs. (D) Spectral responses of I of grating-assisted tip with different NAs.

4 Conclusion

In summary, we presented a method to enhance the nanofocusing characteristic of the plasmonic tip by integrating a grating near the tip apex. Simulation results show that the grating near the tip apex can significantly improve the electric field intensity of the nanofocusing field compared with the conventional bare tip, under axial excitation of the focused RVB. The electric field intensity enhancement characteristic is quantified in relation to the groove number of grating, excitation wavelength, period of grating, and numerical aperture of the MO. These simulation results could be a good reference to fabricate the plasmonic tip for TERS applications and an effective way to promote the development of tip-enhanced near-field optical microscopy.

Acknowledgments: This work was financially supported by the National Natural Science Foundation of China (NSFC) (61675169, 61675171, 91950207, and 11634010, Funder Id: http://dx.doi.org/10.13039/501100001809), National Key R&D Program of China (2017YFA0303800), Natural Science Basic Research Plan in Shaanxi Province of China (2018JM6036), Shaanxi Provincial Key R&D Program (2018KW-009), and Fundamental Research Funds for Central Universities (310201911CX026, and 3102019JC008).

References

[1] Stockle RM, Suh YD, Deckert V, Zenobi R. Nanoscale chemical analysis by tip-enhanced Raman spectroscopy. Chem Phys Lett 2000;318:131–6.
[2] Kurouski D, Deckert-Gaudig T, Deckert V, Lednev IK. Structure and composition of insulin fibril surfaces probed by TERS. J Am Chem Soc 2012;134:13323–9.
[3] Sheng S, Wu JB, Cong X, et al. Vibrational properties of a monolayer silicene sheet studied by tip-enhanced Raman spectroscopy. Phys Rev Lett 2017;119:196803.
[4] Zhang R, Zhang Y, Dong ZC, et al. Chemical mapping of a single molecule by plasmon-enhanced Raman scattering. Nature 2013;498:82–6.
[5] Van Schrojenstein Lantman EM, Deckert-Gaudig T, Mank AJ, Deckert V, Weckhuysen BM. Catalytic processes monitored at the nanoscale with tip-enhanced Raman spectroscopy. Nat Nanotechnol 2012;7:583–6.
[6] Zeng ZC, Huang SC, Wu DY, et al. Electrochemical tip-enhanced Raman spectroscopy. J Am Chem Soc 2015;137:11928–31.
[7] Liu Z, Ding SY, Chen ZB, et al. Revealing the molecular structure of single-molecule junctions in different conductance states by fishing-mode tip-enhanced Raman spectroscopy. Nat Commun 2011;2:305.
[8] Sun MT, Zhang ZL, Chen L, et al. Plasmon-driven selective reductions revealed by tip-enhanced Raman spectroscopy. Adv Mater Interfaces 2014;1:1300125.
[9] Kawata S, Ichimura T, Taguchi A, Kumamoto Y. Nano-Raman scattering microscopy: resolution and enhancement. Chem Rev 2017;117:4983–5001.
[10] Verma P. Tip-enhanced Raman spectroscopy: technique and recent advances. Chem Rev 2017;117:6447–66.
[11] Shi X, Coca-Lopez N, Janik J, Hartschuh A. Advances in tip-enhanced near-field Raman microscopy using nanoantennas. Chem Rev 2017;117:4945–60.
[12] Liao PF, Wokaun A. Lightning rod effect in surface enhanced Raman scattering. J Chem Phys 1982;76:751–2.
[13] Meng L, Sun M. Tip-enhanced photoluminescence spectroscopy of monolayer MoS_2. Photonics Res 2017;5:745–9.
[14] Richard-Lacroix M, Zhang Y, Dong Z, Deckert V. Mastering high resolution tip-enhanced Raman spectroscopy: towards a shift of perception. Chem Soc Rev 2017;46:3922–44.
[15] Wang X, Huang SC, Huang TX, et al. Tip-enhanced Raman spectroscopy for surfaces and interfaces. Chem Soc Rev 2017;46:4020–41.
[16] Stadler J, Schmid T, Zenobi R. Developments in and practical guidelines for tip-enhanced Raman spectroscopy. Nanoscale 2012;4:1856–70.
[17] Lu F, Huang T, Han L, et al. Tip-enhanced Raman spectroscopy with high-order fiber vector beam excitation. Sensors 2018;18:3841.
[18] Schultz ZD, Stranick SJ, Levin IW. Advantages and artifacts of higher order modes in nanoparticle-enhanced backscattering Raman imaging. Anal Chem 2009;81:9657–63.
[19] Kazemi-Zanjani N, Vedraine S, Lagugné-Labarthet F. Localized enhancement of electric field in tip-enhanced Raman spectroscopy using radially and linearly polarized light. Opt Express 2013;21:25271.
[20] Zhang M, Wang J, Tian Q. Tip-enhanced Raman spectroscopy mapping with strong longitudinal field excitation. Opt Commun 2014;315:164–7.
[21] Ropers C, Neacsu CC, Elsaesser T, Albrecht M, Raschke MB, Lienau C. Grating-coupling of surface plasmons onto metallic tips: a nanoconfined light source. Nano Lett 2007;7:2784–8.
[22] Berweger S, Atkin JM, Olmon RL, Raschke MB. Adiabatic tip-plasmon focusing for nano-Raman spectroscopy. J Phys Chem Lett 2010;1:3427–32.
[23] Kim W, Kim N, Park JW, Kim ZH. Nanostar probes for tip-enhanced spectroscopy. Nanoscale 2016;8:987–94.
[24] You Y, Purnawirman NA, Hu H, et al. Tip-enhanced Raman spectroscopy using single-crystalline Ag nanowire as tip. J Raman Spectrosc 2010;41:1156–62.
[25] Taguchi A, Yu J, Verma P, Kawata S. Optical antennas with multiple plasmonic nanoparticles for tip-enhanced Raman microscopy. Nanoscale 2015;7:17424–33.
[26] Vasconcelos TL, Archanjo BS, Fragneaud B, et al. Tuning localized surface plasmon resonance in scanning near-field optical microscopy probes. ACS Nano 2015;9:6297–304.
[27] Maouli I, Taguchi A, Saito Y, Kawata S, Verma P. Optical antennas for tunable enhancement in tip-enhanced Raman spectroscopy imaging. Appl Phys Express 2015;8:032401.
[28] Shen H, Lu G, He Y, Cheng Y, Liu H, Gong Q. Directional and enhanced spontaneous emission with a corrugated metal probe. Nanoscale 2014;6:7512–8.
[29] Qian Q, Yu H, Gou P, Xu J, An Z. Plasmonic focusing of infrared SNOM tip patterned with asymmetric structures. Opt Express 2015;23:12923–34.

[30] Shen H, Lu G, Cao Z, et al. Directionally enhanced probe for side-illumination Tip enhanced spectroscopy. J Raman Spectrosc 2016;47:1194–9.
[31] Johnson PB, Christy RW. Optical constants of the noble metals. Phys Rev B 1972;6:4370–9.
[32] Hermann RJ, Gordon MJ. Quantitative comparison of plasmon resonances and field enhancements of near-field optical antennae using FDTD simulations. Opt Express 2018;26:27668–82.
[33] Zhan Q. Cylindrical vector beams: from mathematical concepts to applications. Adv Opt Photonics 2009;1:1.
[34] Richards B, Wolf E. Electromagnetic diffraction in optical systems. II. Structure of the image field in an aplanatic system. Proc R Soc A: Math Phys 1959;253:358–79.
[35] Youngworth K, Brown T. Focusing of high numerical aperture cylindrical-vector beams. Opt Express 2000;7:77–87.
[36] Novotny L, Stranick SJ. Near-field optical microscopy and spectroscopy with pointed probes. Annu Rev Phys Chem 2006;57:303–31.
[37] Aouani H, Mahboub O, Devaux E, Rigneault H, Ebbesen TW, Wenger J. Plasmonic antennas for directional sorting of fluorescence emission. Nano Lett 2011;11:2400–6.
[38] Lu F, Zhang W, Huang L, et al. Mode evolution and nanofocusing of grating-coupled surface plasmon polaritons on metallic tip. Opto-Electron Adv 2018;1:18001001–7.
[39] Berweger S, Atkin JM, Olmon RL, Raschke MB. Light on the tip of a needle: plasmonic nanofocusing for spectroscopy on the nanoscale. J Phys Chem Lett 2012;3:945–52.
[40] Fang ZY, Lin CF, Ma RM, Huang S, Zhu X. Planar plasmonic focusing and optical transport using CdS nanoribbon. ACS Nano 2010; 4:75–82.
[41] Shan H, Yu Y, Wang X, et al. Direct observation of ultrafast plasmonic hot electron transfer in the strong coupling regime. Light Sci Appl 2019;8:9.
[42] Fang ZY, Peng Q, Song WT, et al. Plasmonic focusing in symmetry broken nanocorrals. Nano Lett 2011;11:893–7.
[43] Bao YJ, Jiang Q, Kang YM, Zhu X, Fang ZY. Enhanced optical performance of multifocal metalens with conic shapes. Light Sci Appl 2017;6:e17071.
[44] Shi H, Wang C, Du C, Luo XG, Dong X, Gao H. Beam manipulating by metallic nano-slits with variant widths. Opt Express 2005;13:6815–20.
[45] Xu T, Du CL, Wang CT, Luo XG. Subwavelength imaging by metallic slab lens with nanoslits. Appl Phys Lett 2007;91:201501.
[46] Luo XG, Tsai DP, Gu M, Hong MH. Subwavelength interference of light on structured surfaces. Adv Opt Photonics 2018;10:757–842.